

Article

High Strain Rate Superplasticity of WE54 Mg Alloy after Severe Friction Stir Processing

Marta Álvarez-Leal ^{1,†}, Fernando Carreño ^{1,*}, Alberto Orozco-Caballero ^{1,‡}, Pilar Rey ² and Oscar A. Ruano ¹

¹ Physical Metallurgy Department, CENIM, CSIC, Av. Gregorio del Amo 8, 28040 Madrid, Spain; m.alvarez@cetemet.es (M.Á.-L.); alberto.orozco.caballero@upm.es (A.O.-C.); ruano@cenim.csic.es (O.A.R.)

² Technological Centre AIMEN, Relva 27A-Torneiros, O'Porriño, 36410 Pontevedra, Spain; prey@aimen.es

* Correspondence: carreño@cenim.csic.es

† Now at Department of R&D and Programmes, Technology Centre of Metal-Mechanical and Transport (CETEMET), Avda. 1° de Mayo, s/n. Linares, 23700 Jaén, Spain.

‡ Now at Department of Mechanical Engineering, Chemistry and Industrial Design, Polytechnic University of Madrid, Ronda de Valencia 3, 28012 Madrid, Spain.

Received: 2 November 2020; Accepted: 23 November 2020; Published: 25 November 2020



Abstract: Friction stir processing (FSP) was used on coarse-grained WE54 magnesium alloy plates of as-received material. These were subjected to FSP under two different cooling conditions, refrigerated and non-refrigerated, and different severe processing conditions characterized by low rotation rate and high traverse speed. After FSP, ultrafine equiaxed grains and refinement of the coarse precipitates were observed. The processed materials exhibited high resistance at room temperature and excellent superplasticity at the high strain rate of 10^{-2} s^{-1} and temperatures between 300 and 400 °C. Maximum tensile superplastic elongation of 726% was achieved at 400 °C. Beyond 400 °C, a noticeable loss of superplastic response occurred due to a loss of thermal stability of the grain size. Grain boundary sliding is the operative deformation mechanism that can explain the high-temperature flow behavior of the ultrafine grained FSP-WE54 alloy, showing increasing superplasticity with increasing processing severity.

Keywords: friction stir processing; WE54 magnesium alloy; superplasticity; grain boundary sliding; processing severity

1. Introduction

Magnesium, as the lightest structural metallic material, is being used in different engineering applications and may replace aluminum once its strength and ductility are improved with the help of intensive research on this material [1,2]. Such investigations will decrease the weight of structures, especially in the automotive and aerospace industries, increasing fuel-efficiency and minimizing its CO₂ footprint.

The strength of magnesium can be increased by alloying with rare earth elements, which usually present high solubility in the magnesium lattice and are effective for precipitation and age hardening [3,4]. This addition can also significantly improve the creep resistance of magnesium alloys, as proven with the addition of yttrium and gadolinium, heavy rare earth (RE) elements that usually improve high temperature strength [3–5].

An additional issue for the widespread use of magnesium comes from its poor workability at room temperature, which makes the fabrication of complex-shaped components a difficult task. This is due to the limited number of slip planes available and the activation of twinning. Such a problem is partially solved by extensive grain refining that may increase ductility at room temperature [6–8].

Among numerous techniques used for achieving ultrafine grain (UFG) microstructures, severe plastic deformation (SPD) processing techniques are nowadays the most promising route [9–11]. The large stresses and huge deformation values imposed during SPD generate high dislocation densities in the materials, which evolve into ultrafine grain structures through recovery and recrystallization processes.

Among the SPD techniques, friction stir processing (FSP) is rapidly developing because it allows the attainment of large products with UFG microstructures and can be easily implemented in the industry. FSP is a versatile solid-state processing technique that can tailor the microstructure and, therefore, the mechanical properties by controlling the processing parameters and the cooling rate. In this work, magnesium samples were friction stir processed under two different cooling conditions, non-refrigerated and cryogenic (liquid nitrogen) cooling, and at various tool rotation and traverse speeds seeking a high severity in the introduction of plastic deformation.

A direct consequence of microstructure refinement is the possibility of deforming in a superplastic way. In such a case, elongations to failure are much larger than for coarse-grained materials, usually reaching values larger than 400%, or 200% for high strain rates ($>10^{-2} \text{ s}^{-1}$) [12]. This behavior is needed for the use of superplastic forming as a feasible production process of geometrically complex parts. In order to make superplastic forming a profitable method at an industrial scale, strain rates equal to or higher than 10^{-2} s^{-1} are required. The underlying deformation mechanism in superplasticity is grain boundary sliding (GBS), which requires a fine grain size, less than 20 μm , and a high fraction of high angle grain boundaries. The grain sliding during GBS requires a diffusion-controlled mechanism that acts as an accommodation process. Therefore, the temperature should be relatively high, which may lead to grain growth as a counter-productive side effect. These two factors should be closely controlled to attain successfully large elongations. In addition, the finer the grain size, the higher the superplastic strain rate, the lower the superplastic temperature, and the slower the grain growth. Therefore, it is interesting to process the material with the highest severity in order to obtain the smallest grain size and benefit from these advantages in the superplastic forming of high added-value structural parts.

2. Material and Experimental Procedure

Extruded WE54 plates of dimensions $300 \times 80 \times 5 \text{ mm}^3$ were received from Magnesium Elektron (Manchester, UK). The plates were solution-heat treated at 525 °C for 8 h, followed by hot water quenching (60 °C) and final aging at 250 °C for 12 h, which consist of the so-called T6 temper [13]. The composition of the alloy was the following (in wt.%): 5% Y–1.5% Nd–1.5% RE–0.45%Zr–balance Mg.

The microstructural characterization was carried out by means of electron back-scattered diffraction (EBSD). EBSD samples were prepared by mechanical polishing up to a final 1 μm diamond particles step, followed by chemical polishing for 5 to 10 s using a solution of 4.2 g picric acid, 10 mL acetic acid, 10 mL H_2O , and 70 mL ethanol.

The as-received plates were subjected to FSP under different processing and cooling conditions. The tool to perform FSP was made of an MP159[®] nickel-cobalt base alloy and it comprises a scrolled shoulder 9.5 mm in diameter and a concentric threaded conical pin with flutes 4.7–4.1 mm in diameter and 1.8 mm in length. The as-received WE54 alloy in the T6 condition was processed by FSP with a special emphasis on high processing severity to obtain the finest possible grain size. In order to achieve the above-mentioned high severity, the material was processed using low rotation rate (ω) and high traverse speed (v) to minimize the heat input (HI), which can be estimated as $\text{HI} \propto \omega^2/v$. Such an approach is convenient for industrial applications, since we decrease the processing time. Furthermore, the sheets were firmly mounted on two different backing plates, one made of steel and the other one made of copper. The latter contains a series of cavities where liquid nitrogen flows to increase the cooling rate. The liquid nitrogen applied flow rate was such that the upper surface of the copper backing anvil reached $-60 \text{ }^\circ\text{C}$, facilitating a high heat extraction during FSP and restricting any possible grain growth. The temperature of the steel backing plate was room temperature. The different

processing conditions, characterized by the traverse speed, v , and the rotational speed, r or ω , and its nomenclature are given in Table 1. The specific cooling conditions are named “refrigerated” and “non-refrigerated” for the copper and steel backing plates, preceded by the letter R or N, respectively.

Table 1. Nomenclatures and values of the friction stir processing (FSP) conditions.

ω (rpm)	v (mm/min)	HI (rpm ² /(mm/min))	Nomenclature
1400	500	3920	N or R14r05v
1000	500	2000	N or R10r05v
1000	1000	1000	N or R10r10v

The six sets of processing conditions, selected following a logarithmic increase in the severity, were named N14r05v, N10r05v, N10r10v, and R14r05v, R10r05v, and R10r10v.

Constant crosshead speed tensile tests (CCST) initially at 10^{-2} s^{-1} were used to characterize the mechanical behavior of the alloy. In addition, strain rate change tests (SRCT) in tension ranging from 10^{-1} to 10^{-5} s^{-1} were performed to characterize the high temperature (300–450 °C) behavior. The tests were performed in air using an Instron 1362 universal testing machine equipped with a four-lamp ellipsoidal furnace. Planar dog-bone tensile samples with $6.5 \times 2 \times 1.7 \text{ mm}$ gage area dimensions were electro-discharge machined so that their longitudinal axis was parallel to the extrusion or FSP direction, as shown in Figure 1. The tensile samples were mirror-polished in their upper surfaces to a final thickness of 1.6 mm to monitor their changes after tensile testing at various temperatures. The true strain, ε , is calculated as $\varepsilon = \ln(1 + e)$, where $e = (l - l_0)/l_0$, l_0 is the initial gage length and l is the instantaneous length. The true stress is defined as $\sigma = F/A_0(1 + e)$, where A_0 is the initial section of the sample and F is the supported load during tensile testing.

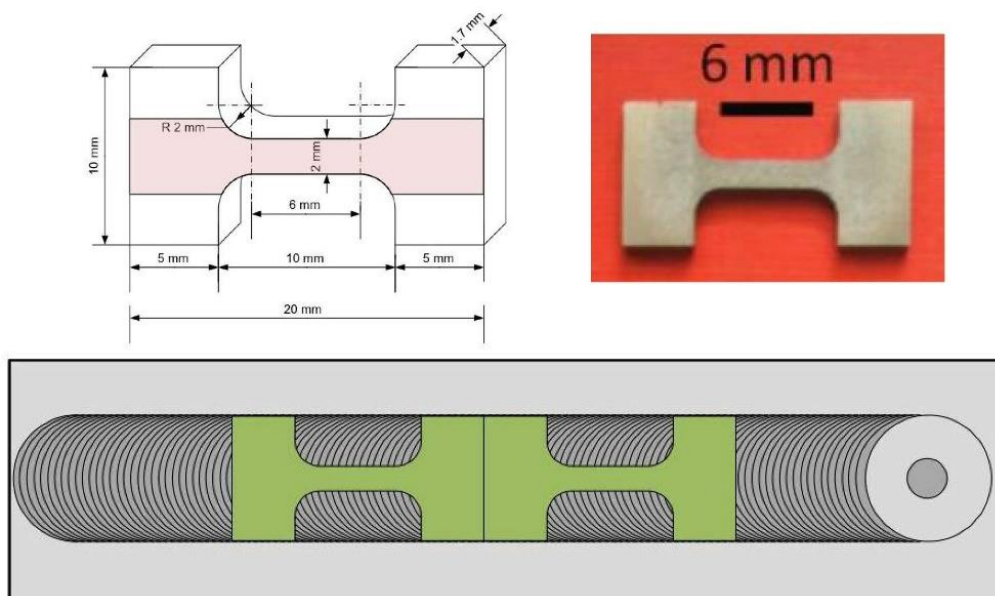


Figure 1. Geometry and orientation of machined tensile samples of the FSPed WE54 Mg alloy.

3. Results

3.1. Microstructures

Figure 2 shows an orientation-imaging map of the as-received WE54 Mg alloy. The micrograph, taken in the L plane, reveals equiaxed grains of diameters in the range 50 to 250 μm . A description of similar microstructures is given elsewhere [14–16].

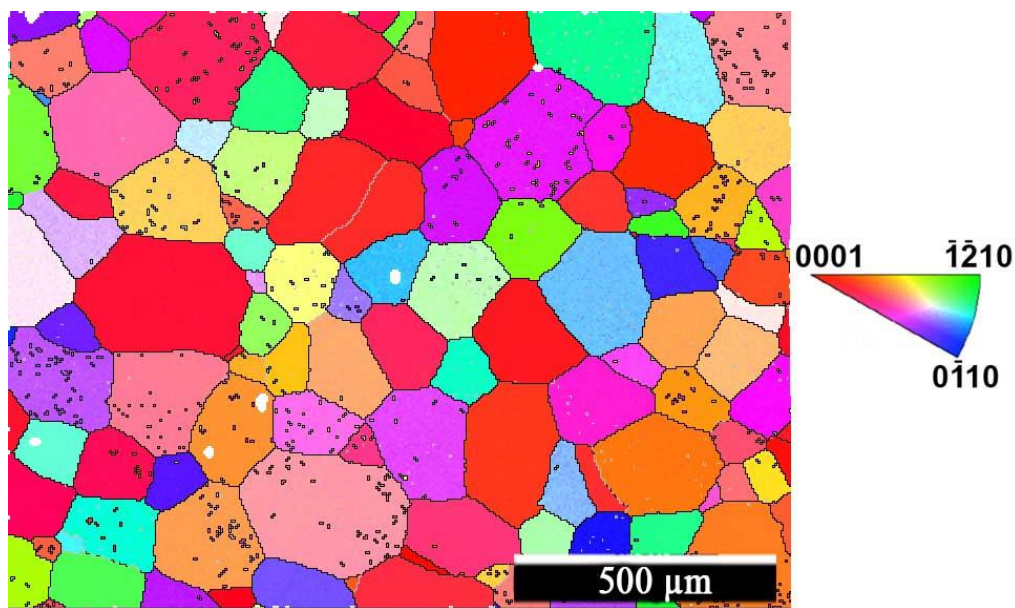


Figure 2. Orientation-imaging map (OIM) obtained by electron back-scattered diffraction (EBSD) of the as-received WE54 Mg alloy, T6 condition.

Figure 3 shows orientation-imaging maps of the WE54 alloy (EBSD inverse pole figure maps) after FSP of the 10r10v material, (a) non-refrigerated and (b) refrigerated.

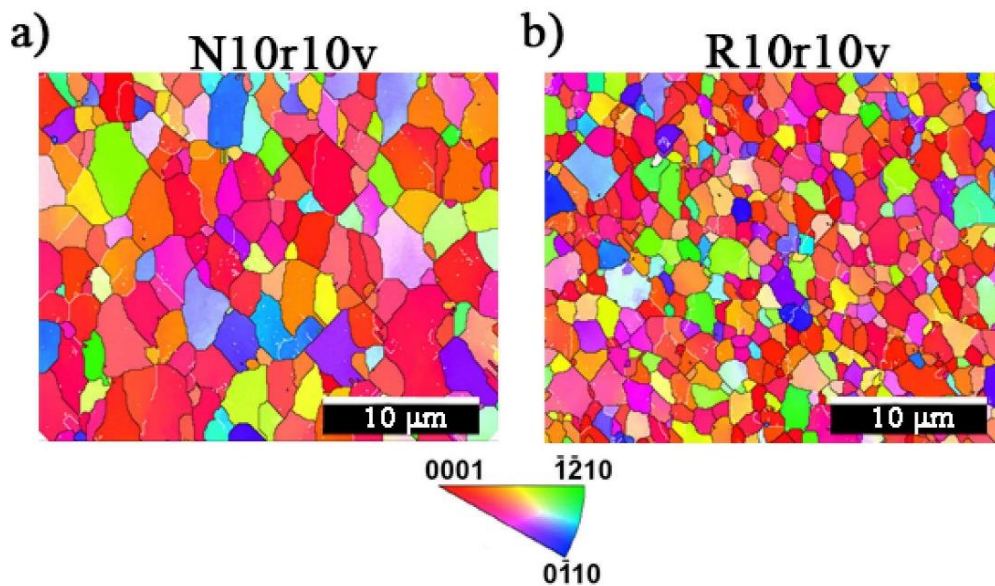


Figure 3. Orientation-imaging maps of the WE54 alloy (EBSD inverse pole figure maps) after FSP in the conditions (a) N10r10v and (b) R10r10v.

The grain size values of the R10r10v and N10r10v materials, which correspond to the most severe FSP condition, measured by Feret diameters, are 0.9 and 1.3 μm , respectively. As is evident from comparing Figures 2 and 3 (please note the different scale, 500 vs. 10 μm), a huge refinement has been attained by severe processing of this magnesium alloy.

3.2. Tensile Tests to Rupture of WE54 Alloy Processed by FSP

Figure 4 shows stress–strain curves at initial strain rates of 10^{-2} s^{-1} and various temperatures of the WE54 alloy processed by FSP under three processing conditions and two cooling conditions, refrigerated

and non-refrigerated. Two different behaviors can be distinguished, one at low (high stresses and low ductility) and another one at high (low stresses and high ductility) temperatures, with a transition temperature around 250–300 °C. The low temperature regime (25–200 °C) shows very similar low tensile ductility values < 25% for all samples and high stress values, which decrease slightly with increasing temperature in this interval. On the contrary, the high temperature interval (350–450 °C) shows very large tensile elongations (as high as 726%), and very low stress values. This contrast between low and high temperature behavior increases with increasing processing severity and with the use of refrigeration. The transition temperatures (250–300 °C) are also affected by refrigeration and processing severity. For the non-refrigerated conditions, at 300 °C the ductility values increase noticeably with increasing severity, while for the refrigerated conditions, the increasing ductility is observed from 250 °C for the two most severe processing conditions. Additionally, the largest tensile ductility value is observed for all conditions at 400 °C, accompanied by very low stress values. At 450 °C, the stress values increase and the ductility values drop, which indicates changes in the deformation mechanism.

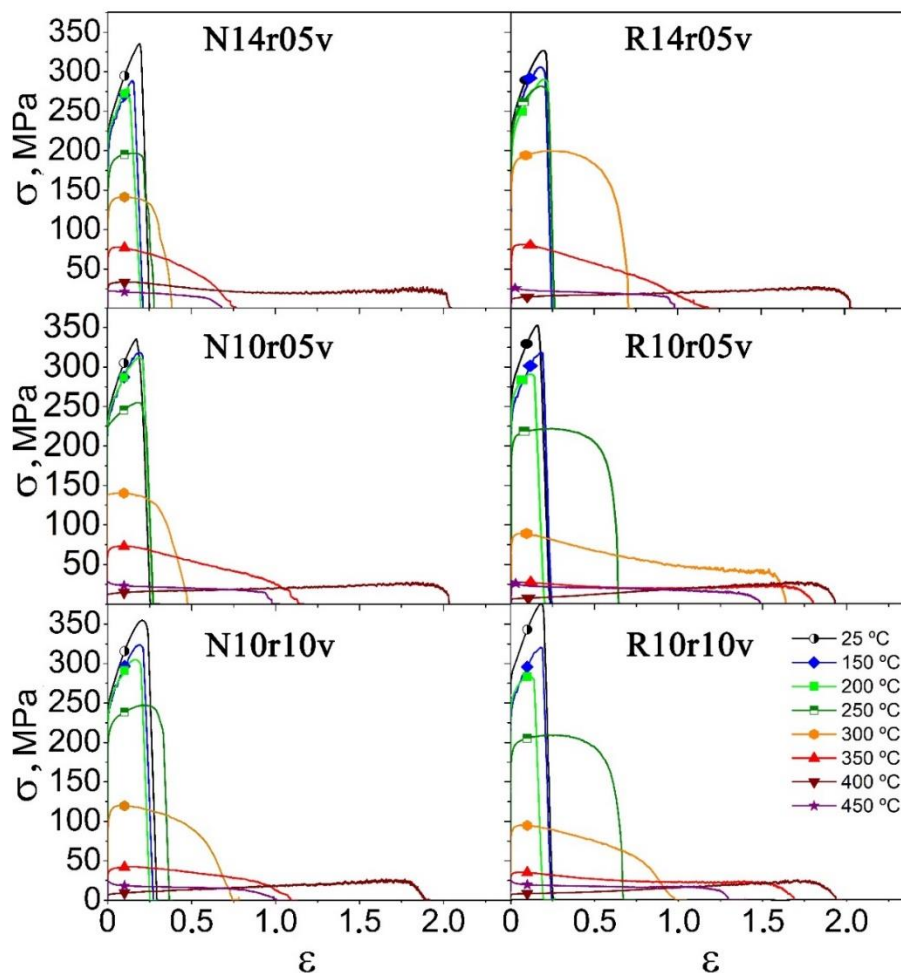


Figure 4. Stress–strain curves of materials processed by FSP and tested at an initial strain rate of 10^{-2} s^{-1} at temperatures from 25 to 450 °C, non-refrigerated (N, left) and refrigerated (R, right).

Table 2 gives the mechanical parameters of all the curves presented in Figure 4. It is remarkable the high elongation values reached at 400 °C for all materials under all conditions at this high strain rate. A maximum elongation to failure of 726% is observed for the R14r05v material. Nonetheless, very high values of 562, 593, 599, 664, and 666% are also obtained for the rest of the conditions at 400 °C. It is also interesting to note that very high elongations are also obtained at 350 °C and in some

conditions at 300 and 450 °C. However, at 450 °C, there is a clear loss of ductility with respect to 400 °C, which is attributed to massive grain growth, and will be discussed in depth in the next section.

Table 2. Yield stress ($\sigma_{0.2}$), flow stress (σ), uniform elongation (e_u), and elongation to failure (e_F) at different test temperatures of the alloy WE54 processed by FSP and tensile tested at 10^{-2} s^{-1} .

Condition	T (°C)	$\sigma_{0.2}$ (MPa)	σ (MPa)	e_u (%)	e_F (%)
N14r05v	20	195	335	21	22
	150	165	288	15	17
	200	205	281	13	14
	250	146	197	18	24
	300	111	141	12	46
	350	63	78	7	107
	400	26	33	17	666
	450	21	22	2	98
	N10r05v	20	220	336	19
150		213	318	22	24
200		218	312	21	24
250		224	255	21	26
300		138	140	8	61
350		60	73	8	210
400		12	17	69	664
450		26	28	1	166
N10r10v		20	230	355	23
	150	223	324	21	24
	200	219	305	18	22
	250	194	247	23	39
	300	90	120	7	107
	350	32	43	14	198
	400	6	14	76	562
	450	22	24	1	169
	R14r05v	20	203	327	22
150		194	306	20	23
200		179	290	21	25
250		195	282	20	25
300		148	200	26	101
350		60	81	6	226
400		16	23	10	726
450		20	23	3	222
R10r05v		20	248	354	17
	150	213	282	13	14
	200	231	292	13	15
	250	179	223	27	89
	300	71	90	7	420
	350	23	28	7	512
	400	6	15	96	599
	450	29	30	0.4	345
	R10r10v	20	270	375	20
150		209	319	19	21
200		230	283	11	15
250		159	209	25	94
300		75	94	8	166
350		26	35	7	440
400		6	12	97	593
450		22	23	0.6	265

Figure 5 shows curves of the elongation to failure at 10^{-2} s^{-1} as a function of temperature for the WE54 alloy after FSP under various conditions. For comparison, data from the as-received material in the T6 condition (not subjected to FSP) are included in the figure [17]. The ductility continuously increases with temperature and a strong peak is observed at 400 °C. At this temperature, the ductility values for all samples are around 700% with a maximum of 726% observed in the R14r05v material. It can also be observed that at 250–350 °C, the tensile ductility values of the refrigerated conditions (continuous lines) are higher than those corresponding to the non-refrigerated ones (dashed lines).

At 450 °C, the elongation to failure drastically drops, pointing to a change in the deformation mechanism as a result of grain growth. This peak and the subsequent drop do not exist in the non-processed WE54 material, since the ductility increases continuously up to the highest temperature of 450 °C [17].

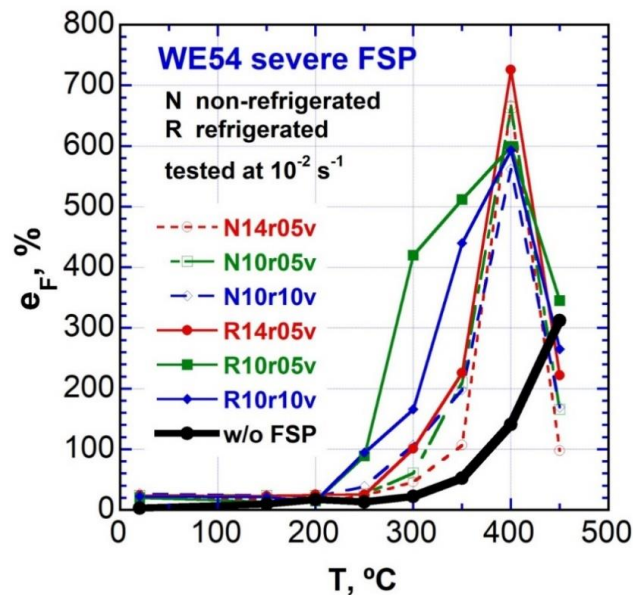


Figure 5. The elongation to failure as a function of temperature for the FSP WE54 alloy tested at 10^{-2} s^{-1} .

Very low stress values are also observed at high temperatures in most of the tensile tests in the range 350–450 °C. The flow stress, σ , as a function of temperature at 10^{-2} s^{-1} , is represented in Figure 6. Again, for comparison, data from the as-received material in the T6 condition (not subjected to FSP) are included in the figure [17]. The figure shows a moderate decrease in the stress with temperature up to 200 °C. Above this temperature, the stress strongly drops. The same behavior is observed for all FSP and cooling conditions. The highest stress value at room temperature is given for the material processed under the most severe condition, and refrigerated, R10r10v. On the contrary, at high temperatures, this material shows the lowest stress values. It should be noted the slight stress increase at 450 °C, which is attributed to rapid grain coarsening of all our WE54 processed materials at such a high temperature. This behavior can be compared with that of the material without FSP [17], for which the increase at 450 °C does not exist and the curve continuously decreases from 250 °C.

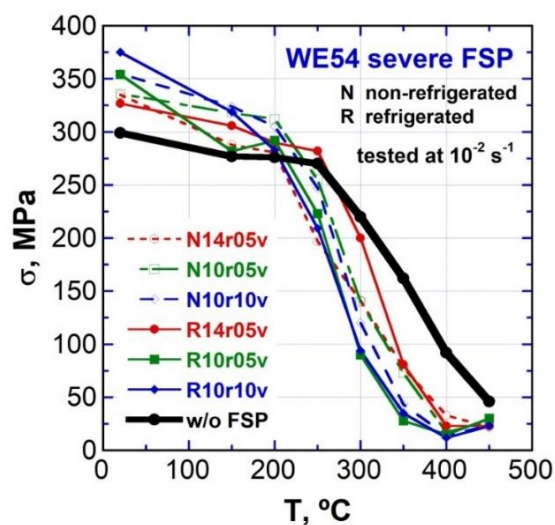


Figure 6. The flow stress as a function of temperature for the FSP WE54 alloy tested at 10^{-2} s^{-1} .

3.3. Surface Morphology of Samples after the Constant Strain Rate Tests

The surface morphology of the tested samples gives a clear hint of the underlying microstructures, especially under superplastic conditions for which sliding of the grains is clearly visible. Figure 7 presents those SEM micrographs after testing at 10^{-2} s^{-1} for the 14r05v materials under the two cooling conditions. Similar microstructures are obtained for the other two processing conditions, 10r05v and 10r10v. Fine grains are depicted in all cases except at 450 °C. Before testing, the Feret diameters were about 0.9 and 1.3 μm for the refrigerated and non-refrigerated materials, respectively. These grain sizes are similar to those tested at 250 °C, for which deformation is small. Larger grains are observed in samples deformed at higher temperatures attesting grain growth during testing. At 350–400 °C, clear hints of grain boundary sliding are observed with the grains sliding against each other, as shown in Figure 7. This fine microstructure is able to attain very large elongations, 726% at 400 °C, at high strain rate, as shown in Figure 5. At 450 °C, the microstructure is unstable, tending to grow quickly so that most of the grains become too large to withstand superplastic deformation for most of the FSPed microstructures.

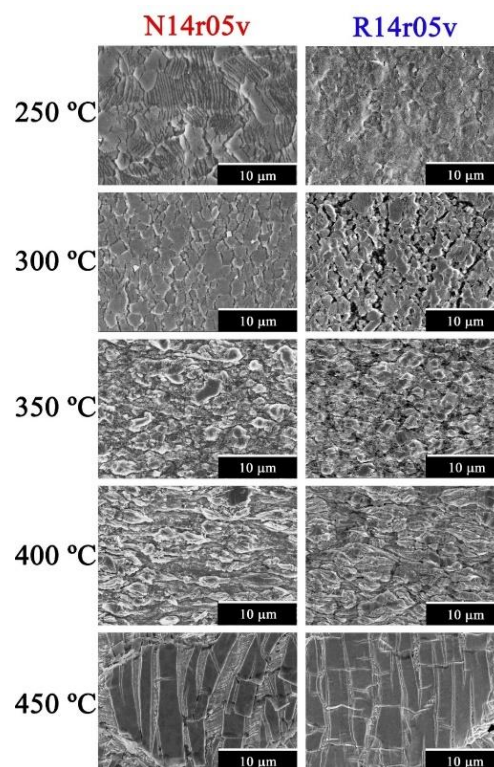


Figure 7. SEM micrographs of the topography of samples tested at 10^{-2} s^{-1} at various temperatures for the processing condition 14r05v, non-refrigerated (N, left) and refrigerated (R, right).

3.4. Strain Rate Change Tests

Figure 8 shows data from the strain rate change tests performed in the range 300 to 450 °C at strain rates from 10^{-5} to 10^{-1} s^{-1} for all processing conditions and two cooling conditions. The slope of the curves corresponds to the apparent stress exponent, n . A low n value of about 2 is usually observed at low strain rates and high temperature, which is typical of superplastic materials where grain boundary sliding controls deformation. The increase to higher n values at high strain rates and lower temperatures in these materials is usually attributed to a change into slip creep as the controlling deformation mechanism. As observed in Figure 8, there is a gradual decrease in stress values (from as high as 200 MPa at 300 °C to as low as 1–2 MPa at 400 °C) and n values (towards 2 at 400 °C) with increasing testing temperature, for all samples. At 350–400 °C, there is a wide interval of high strain

rates for which the FSPed alloys show low n values close to two, which can be associated to GBS of the ultrafine grains. Although the high temperature behavior of the different samples appears to be quite similar, some hints show that there is an influence of the processing severity and refrigeration on the superplastic response, which will be highlighted in the discussion section. The anomalous behavior at 450 °C is noticeable, for which their stress values should be lower than those of 400 °C; however, most of them are even higher.

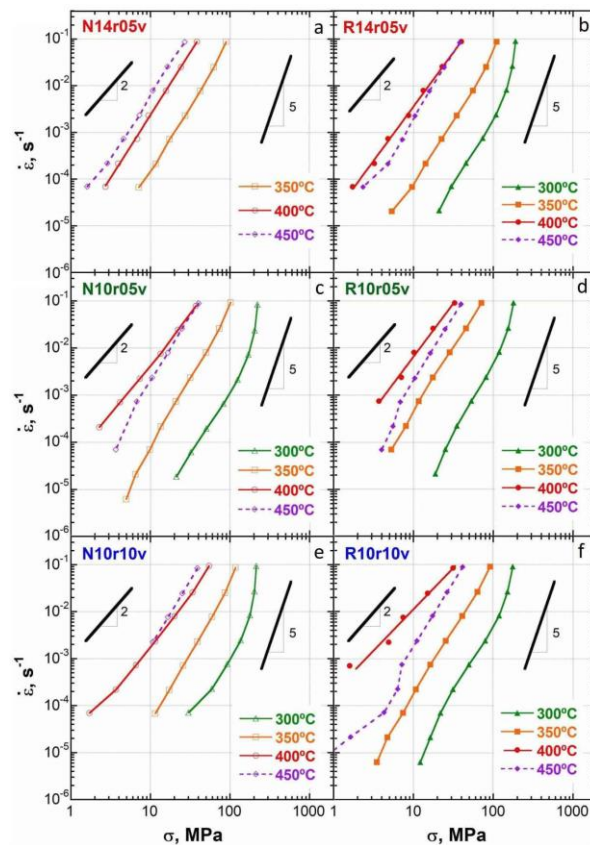


Figure 8. (a–f) Strain rate as a function of stress obtained by strain rate change tests for the six FSP processing conditions, non-refrigerated (N, left) and refrigerated (R, right).

Regarding the activation energy, only an estimation can be provided since there is no constant value of stress exponent and the microstructure is constantly coarsening. For instance, a rough evaluation has been made in the R14r05v material between 300 and 400 °C at 40 MPa, in the range of low n values, that gives a value of about 180 kJ/mol, somewhat higher than the activation energy value associated with lattice diffusion, Q_L . However, negatives values (without any physical meaning) are found when trying to obtain an activation energy value between 400 and 450 °C, associated with a change in the deformation mechanism.

4. Discussion

The present study makes evident the need to understand the influence of FSP conditions and the resulting microstructure on the wide range of deformation behaviors of the materials processed at different rates and cooling conditions. Figure 6 shows the high resistance at low temperatures, which is a result of the severe grain refinement due to the strategy of imposing high severity processing conditions. This is reached by a combination of low rotation speed, minimizing the frictional heat generation, and by increasing the traverse speed to ease a quick heat dissipation, minimizing the process temperature and reducing grain growth just after the tool pass [18–20]. The Hall–Petch law predicts an increase in the stress with decreasing grain size, at low temperature, as occurs for the

processed material, but other factors such as the grain size distribution, refinement of the second phases, and the presence of elements in solid solution may also influence this behavior [21]. On the other hand, the figure also shows the rapid decrease in the stress above 250 °C for all materials, and especially, in the processed materials. This rapid stress drop with increasing temperature is attributed to the start of a creep behavior that is mainly controlled by diffusional processes. These diffusional processes generally involve the ability of dislocations to bypass the obstacles. These obstacles are usually overcome through a climb mechanism, but, in the presence of solutes, an interaction among dislocations and solutes may be controlling as well. Additionally, when the material presents small, equiaxed, and highly misoriented grains, another diffusional mechanism may take control of the creep behavior under certain strain rate and temperature conditions, which is GBS in the so-called superplastic window. The three possible mechanisms differ in their microstructural evolution, and stress and ductility values at high temperature. The solid solution creep mechanism brings higher stresses due to the reinforcing solute–dislocation interactions, and showing elongated grains parallel to the imposed deformation. On the contrary, the GBS mechanism yields easy deformation at much lower stresses than those of dislocation-based creep mechanisms and the morphology of grains does not change even after very large deformations, remaining equiaxed and highly misoriented. The ductility obtained by GBS is usually much higher than for any other mechanism, in parallel to the much lower creep stresses measured during high temperature deformation. Additionally, the smaller the grain size, the larger the ductility, the lower the creep stress, and the higher the strain rate sustaining GBS. This is the reason underlying our strategy to process the material severely, in order to obtain the finest microstructure as possible [18–20].

As shown clearly in Figure 6, the six processed materials present much lower stress values than those of the as-received WE54 magnesium alloy, at high temperature, up to a minimum value at 400 °C. The stress values can be as low as a factor of four, which is very useful for the industrial forming of complex parts. This behavior corresponds to a different deformation mechanism than that operating in the non-processed as-received alloy.

Another feature important to note in Figure 6 is the increase in the stress at 450 °C in the FSP materials at which the microstructure coarsens significantly (Figure 7). Therefore, the mechanism controlling deformation at high temperature is one depending on grain size. In contrast, the material not subjected to FSP does not show such behavior which is an indication that, at high temperature, the controlling mechanism is different from that of the processed materials. Indeed, the behavior of the as-received material was attributed to a solute-drag slip creep mechanism [17,22], as a rate-controlling process which is grain size-independent. Correspondingly, Figure 5 clearly shows the rapid increase in the elongation to failure from 20 to 400 °C and their high values, much higher than those corresponding to the as-received material, up to about 700%, typical of a grain boundary sliding mechanism for which the ductility is sensibly dependent on grain size [23–25].

In addition, a homogeneous equiaxed microstructure is present after deformation, up to 400 °C, as shown in Figure 7, and a low stress exponent, close to 2, is obtained, as shown in Figure 8. This figure also shows very low stress values, which corroborate the strong decrease in stresses above 300 °C shown in Figures 6 and 8. This evidence points clearly to the grain boundary sliding mechanism as the one controlling deformation. The high strain rates where n is still close to 2 at temperatures above 300 °C are remarkable. This wide range of strain rates is associated to the fine grain size obtained by severe friction stir processing of the WE54 Mg alloy, around 1 μm at the start of testing. At 300 °C and above 10^{-2} s^{-1} , a typical power law region is observed with n values higher than 5, pointing to a dislocation creep mechanism at lower temperatures. At 450 °C, for which the microstructure strongly coarsens, as revealed in Figure 7, a change back to a dislocation creep mechanism is taking place.

The various graphs of Figure 8 from strain rate change tests corresponding to the six processed materials show similar behavior. A relatively large range of strain rates and temperatures is found, where n is about 2 and, therefore, superplastic properties can be expected in such a large window, even at strain rates as high as 10^{-1} s^{-1} at the highest temperatures. This behavior corresponds to a

GBS mechanism, as the processed alloys possess ultrafine, equiaxed, and highly misoriented grains, the stresses are low, and the ductility values are very high. In the range of low temperature and high strain rates, a change towards dislocation creep is observed, increasing the values of the stress exponent, as expected, and corroborated by Figure 6, as well. Another interesting feature revealed in these graphs is the behavior at 450 °C. As grain coarsening is taking place rapidly during testing at this temperature in the processed alloys, the stresses are higher than expected, and they even cross the lines corresponding to the data at 400 °C, showing higher stress exponents. In fact, as shown in Figure 8c,d,f, there is an abrupt change in slope at 450 °C at low strain rates because increasing coarsening is leading the behavior of the ultrafine processed alloy towards the behavior corresponding to a coarse-grained alloy. Effectively, the solute-drag slip creep mechanism, characterized by a stress exponent of 3, was demonstrated to occur in the same WE54 material that was not severely plastically deformed by FSP and had a coarse grain size [17]. Since the sample tested at 450 °C showed large grain growth, it is reasonable to assume that the sample is in the process of changing mechanisms from GBS to solute-drag creep. This is especially important during deformation at the lowest strain rates, where the sample remains at this temperature for a long time. Due to the continuous grain coarsening at high temperature, even extreme at 450 °C, leading to a change in deformation mechanism, it is difficult to obtain a true activation energy value associated with the high temperature creep of the processed alloys. In the range 300–400 °C, an approximate value of 180 kJ/mol is obtained for the activation energy for creep in the R14r05v material, although in the range 400–450 °C, the value becomes negative, without physical meaning, due to the change in deformation mechanism. Temperature-dependent activation energy values were also found for a similar fine-grained Mg–Y–Nd alloy [26]. However, the value obtained, although slightly high, is not far from that corresponding to lattice self-diffusion of magnesium, 135 kJ/mol [27,28], and may be regarded as typical of reinforced magnesium alloys. In summary, between 300 and 400 °C, the materials deform by a GBS mechanism and at 450 °C, the ultrafine-grained alloys coarsen their microstructures rapidly and change their superplastic behavior towards a solute drag creep mechanism, as the initial, unprocessed coarse WE54 alloy [17].

Figure 9 gives a comparison of the curves at 300 and 400 °C between the two cooling conditions, non-refrigerated and refrigerated, for the N10r10v and R10r10v materials. It is observed that the refrigerated material, the most severely processed one, is less resistant at both temperatures, which is a result of the finest grain size obtained. This means that at 300 °C, there is already an influence of grain size on stress values, corroborated by Figure 6. Additionally, the ductility values are also much higher for the processed alloys than for the unprocessed initial WE54, as observed in Figure 5, at 300 °C, thus showing that it is at about this temperature from which the start of deformation controlled by grain boundary sliding can be attributed.

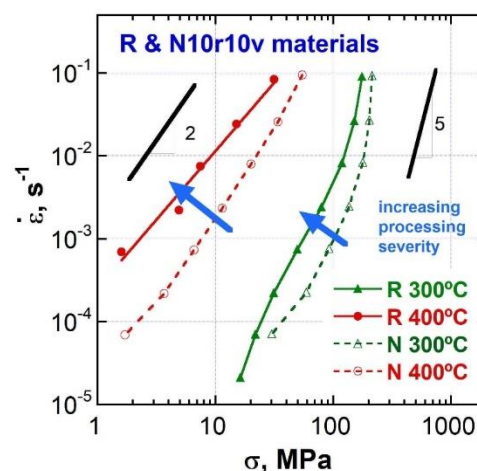


Figure 9. Comparison of FSP WE54 10r10v materials, refrigerated (R) and non-refrigerated (N).

An important aspect that influences the creep behavior of FSP materials is the severity of the processing. Figure 10 shows strain rate versus stress curves at 400 °C for the refrigerated materials with different processing conditions. As mentioned before, the severity of the processing increases following the order $14r05v < 10r05v < 10r10v$. The figure shows that the stress decreases at an imposed strain rate, or conversely, the strain rate at a given stress increases in the same order, according to the applied processing severity. This favors the forming process, which is a consequence of the microstructure refining with increasing severity. Therefore, it can be concluded that processing severity is an important factor that influences the creep behavior of the WE54 magnesium alloy by achieving ultrafine grain sizes which allow for superplasticity at higher strain rates. Similarly, a low heat input applied to a Mg-9Li-1Zn alloy has also been successful to obtain ultrafine grains [29]. Furthermore, the ultrafine grain sizes obtained also improve the resistance of the WE54 alloy at room temperature.

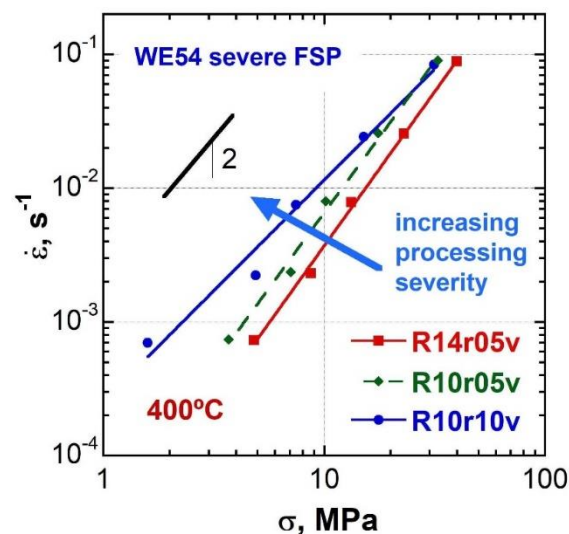


Figure 10. The strain rate as a function of stress at 400 °C for the refrigerated materials with different processing conditions to show the influence of the processing severity.

5. Conclusions

1. Friction stir processing under highly severe conditions was successfully applied to the coarse WE54 alloy, so that refinement of the coarse precipitates and fine equiaxed grains was obtained.
2. The processed materials showed fine grains of the order of 1 μm and exhibited excellent high strain rate superplasticity at temperatures between 300 and 400 °C, and strain rates even higher than 10^{-2} s^{-1} . This behavior contrasts with the higher resistance and lower ductility of the unprocessed WE54 Mg alloy.
3. Large elongations, with a maximum of 726%, were achieved at 400 °C and 10^{-2} s^{-1} . Additionally, low stress and stress exponent values associated with grain boundary sliding are obtained, which were lower the higher the processing severity. Beyond 400 °C, the elongations rapidly decreased as a consequence of microstructure coarsening.
4. At 450 °C, a transition of mechanisms occurs from grain boundary sliding to solute drag creep as the microstructure coarsens. This last mechanism is the operative mechanism of the coarse unprocessed alloy at high temperatures.
5. Severe friction stir processing has been proven to be a method of obtaining ultrafine grains in Mg alloys and, thus, producing materials of high resistance at low temperatures, and easy to form superplastically at high temperatures and high strain rates.

Author Contributions: Conceptualization and methodology, F.C. and O.A.R.; investigation, M.Á.-L., F.C. and O.A.R.; data curation and visualization, M.Á.-L., F.C. and O.A.R.; supervision: A.O.-C., F.C. and O.A.R.; sample manufacturing by FSP, M.Á.-L. and P.R.; material characterization, M.Á.-L.; writing—original draft preparation, O.A.R. and F.C.; writing—review and editing, O.A.R., M.Á.-L., A.O.-C. and F.C.; resources, funding acquisition, and project administration, F.C. and P.R. All authors have read and agreed to the published version of the manuscript.

Funding: Project MAT2015-68919-R MINECO/FEDER, Spain, and FPI fellowship number BES2013-063963 (MINECO/FEDER/ESF).

Acknowledgments: Financial support from MINECO (Spain), Project MAT2015-68919-R (MINECO/FEDER) is gratefully acknowledged. A.O.-C. also thanks CENIM, CSIC, for a contract funded by the aforementioned project. M.Á.-L. thanks MINECO for a FPI fellowship, number BES2013-063963 (MINECO/FEDER/ESF).

Conflicts of Interest: The authors declare no conflict of interest.

References

1. Mordike, B.L.; Ebert, T. Magnesium: Properties—Applications—Potential. *Mater. Sci. Eng. A* **2001**, *302*, 37–45. [[CrossRef](#)]
2. Luo, A.A. Recent Magnesium Alloy Development for Elevated Temperature Applications. *Int. Mater. Rev.* **2004**, *49*, 13–30. [[CrossRef](#)]
3. Bettles, C.; Gibson, M.; Zhu, S. Microstructure and Mechanical Behaviour of an Elevated Temperature Mg-Rare Earth Based Alloy. *Mater. Sci. Eng. A* **2009**, *505*, 6–12. [[CrossRef](#)]
4. Tekumala, S.; Seetharaman, S.; Almajud, A.; Gupta, M. Mechanical Properties of Magnesium-Rare Earth Alloy Systems: A Review. *Metals* **2015**, *5*, 1–39. [[CrossRef](#)]
5. Maruyama, K.; Suzuki, M.; Sato, H. Creep Strength of Magnesium-Based Alloys. *Metall. Mater. Trans.* **2002**, *33*, 875–882. [[CrossRef](#)]
6. Kaibyshev, O.A.; Kazachkov, I.V.; Salikhov, S.Y.A. The Influence of Texture on Superplasticity of the Zn-22% Al Alloy. *Acta Metall.* **1978**, *26*, 1887–1894. [[CrossRef](#)]
7. McFadden, S.X.; Mishra, R.S.; Valiev, R.Z.; Zhilyaev, A.P.; Mukherjee, A.K. Low-Temperature Superplasticity in Nanostructured Nickel and Metal Alloys. *Nature* **1999**, *398*, 684–686. [[CrossRef](#)]
8. Fukusumi, M.; Somekawa, H.; Mukai, T. Texture and Mechanical Properties of a Superplastically Deformed Mg-Al-Zn Alloy Sheet. *Scripta Mater.* **2009**, *61*, 883–889.
9. Kawasaki, M.; Langdon, T.G. Review: Achieving Superplastic Properties in Ultrafine-Grained Materials at High Temperatures. *J. Mater. Sci.* **2015**, *51*, 19–32. [[CrossRef](#)]
10. Alizadeh, R.; Mahmudi, R.; Ngan, A.H.W.; Pereira, P.H.R.; Huang, Y.; Langdon, T.G. Microstructure, Texture, and Superplasticity of a Fine-Grained Mg-Gd-Zr Alloy Processed by Equal-Channel Angular Pressing. *Metall. Mater. Trans. A* **2016**, *47*, 6056–6069. [[CrossRef](#)]
11. Kim, Y.S.; Kim, W.J. Microstructure and Superplasticity of the as-Cast Mg-9Al-1Zn Magnesium Alloy after High-Ratio Differential Speed Rolling. *Mater. Sci. Eng. A* **2016**, *677*, 332–339. [[CrossRef](#)]
12. *Glossary of Terms Used in Metallic Superplastic Materials*; JIS H 7007; Japanese Standards Association: Tokyo, Japan, 1995.
13. Nie, J.F.; Muddle, B.C. Characterisation of Strengthening Precipitate Phases in a Mg-Y-Nd Alloy. *Acta Mater.* **2000**, *48*, 1691–1703. [[CrossRef](#)]
14. Antion, C.; Donnadieu, P.; Perrard, F.; Deschamps, A.; Tassin, C.; Pisch, A. Hardening Precipitation in a Mg-4Y-3RE Alloy. *Acta Mater.* **2003**, *51*, 5335–5348. [[CrossRef](#)]
15. Kiebus, A. The Influence of Ageing on Structure and Mechanical Properties of WE54 Alloy. *J. Achiev. Mater. Manuf. Eng.* **2007**, *23*, 27–30.
16. Liu, H.; Zhu, Y.M.; Wilson, N.C.; Nie, J.F. On the Structure and Role of β'_F in β_1 Precipitation in Mg-Nd Alloys. *Acta Mater.* **2017**, *133*, 408–426. [[CrossRef](#)]
17. Ruano, O.A.; Álvarez-Leal, M.; Orozco-Caballero, A.; Carreño, F. Large Elongations in WE54 Magnesium Alloy by Solute-Drag Creep Controlling the Deformation Behavior. *Mater. Sci. Eng. A* **2020**, *791*, 139757. [[CrossRef](#)]

18. Orozco-Caballero, A.; Cepeda-Jiménez, C.M.; Hidalgo-Manrique, P.; Rey, P.; Gesto, D.; Verdera, D.; Ruano, O.A.; Carreño, F. Lowering the Temperature for High Strain Rate Superplasticity in an Al-Mg-Zn-Cu Alloy via Cooled Friction Stir Processing. *Mater. Chem. Phys.* **2013**, *142*, 182–185. [[CrossRef](#)]
19. Orozco-Caballero, A.; Hidalgo-Manrique, P.; Cepeda-Jiménez, C.M.; Rey, P.; Verdera, D.; Ruano, O.A.; Carreño, F. Strategy for Severe Friction Stir Processing to Obtain Acute Grain Refinement of an Al-Zn-Mg-Cu Alloy in Three Initial Precipitation States. *Mater. Charact.* **2016**, *112*, 197–205. [[CrossRef](#)]
20. Orozco-Caballero, A.; Ruano, O.A.; Rauch, E.F.; Carreño, F. Severe Friction stir Processing of an Al-Zn-Mg-Cu Alloy: Misorientation and Its Influence on Superplasticity. *Mater. Design* **2018**, *137*, 128–139. [[CrossRef](#)]
21. Chiang, C.R. The Grain Size Effect on the Flow Stress of Polycrystals. *Scripta Metall.* **1985**, *19*, 1281–1283. [[CrossRef](#)]
22. Taleff, E.M.; Henshall, G.A.; Nieh, T.G.; Lesuer, D.R.; Wadsworth, J. Warm-Temperature Tensile Ductility in Al-Mg Alloys. *Metall. Mater. Trans. A* **1998**, *29*, 1081–1091.
23. Ruano, O.A.; Miller, A.K.; Sherby, O.D. The Influence of Pipe Diffusion on the Creep of Fine-Grained Materials. *Mater. Sci. Eng.* **1981**, *51*, 9–16. [[CrossRef](#)]
24. Langdon, T.G. The Mechanical Properties of Superplastic Materials. *Mater. Trans. A* **1982**, *13*, 689–701. [[CrossRef](#)]
25. Ruano, O.A.; Sherby, O.D. On Constitutive Equations for Various Diffusion-Controlled Creep Mechanisms. *Revue Phys. Appl.* **1988**, *23*, 625–637. [[CrossRef](#)]
26. Vavra, T.; Minarik, P.; Vesely, J.; Kral, R. Excellent Superplastic Properties Achieved in Mg-4Y-3RE Alloy in High Strain Rate Regime. *Mater. Sci. Eng. A* **2020**, *784*, 139314. [[CrossRef](#)]
27. Shewmon, P.G.; Rhines, F.N. Rate of Self-Diffusion in Polycrystalline Magnesium. *JOM* **1954**, *6*, 1021–1025. [[CrossRef](#)]
28. Frost, H.J.; Ashby, M.F. *Deformation-Mechanism Maps*, 1st ed.; Pergamon Press: Oxford, UK, 1982; p. 44.
29. Zhou, M.; Morisada, Y.; Fujii, H.; Wang, J.-Y. Pronounced Low-Temperature Superplasticity of Friction Stir Processed Mg-9Li-1Zn Alloy. *Mater. Sci. Eng. A* **2020**, *780*, 139071. [[CrossRef](#)]

Publisher’s Note: MDPI stays neutral with regard to jurisdictional claims in published maps and institutional affiliations.



© 2020 by the authors. Licensee MDPI, Basel, Switzerland. This article is an open access article distributed under the terms and conditions of the Creative Commons Attribution (CC BY) license (<http://creativecommons.org/licenses/by/4.0/>).